Extreme deep-sea warmth supports high climate sensitivity in the early Eocene hothouse

Authors: Tobias Agterhuis[1*], Martin Ziegler[1], & Lucas J. Lourens[1]

Affiliations: [1]Department of Earth Sciences, Faculty of Geosciences, Utrecht University, Utrecht, the Netherlands

*Corresponding author. Email: t.agterhuis@uu.nl.

The early Eocene (56–48 Ma) hothouse experienced the highest CO_2 levels of the Cenozoic, as well as the occurrence of multiple transient global warming events, so-called hyperthermals. The deep ocean constitutes a stable and vast heat reservoir in the climate system, and hence compromises a robust setting to estimate past global mean temperatures. However, available deep-sea temperature reconstructions rely on uncertain assumptions of non-thermal influences. Here, we apply for the first time the carbonate clumped isotope paleothermometer (Δ_{47}), a proxy not governed by these uncertainties, on early Eocene benthic foraminifera to evaluate South Atlantic deep-sea temperatures across two hyperthermal events (ETM2 and H2; ~54 Ma). In comparison to the conventional $\delta^{18}O$-based estimates, our new temperature reconstructions indicate two and a half degrees warmer deep water conditions, i.e. 13.2±1.9 °C (95% Confidence Interval) for background state, and average deep-sea warming of 3.3±2.9 °C (95% CI) during these hyperthermal events. These findings imply a reassessment of the assumed isotope composition of the ancient seawater and of a potential pH effect on foraminiferal oxygen isotopes. On a broad scale, our Δ_{47}-based overall warmer deep-sea temperatures provide new evidence for high climate sensitivity during the early Eocene hothouse.

A potential analogue for the future climate state is the extremely warm climate of the early Eocene (56–48 Ma)[1–3], a period in the Cenozoic when ice sheets were absent and CO_2 levels were much higher than today (~600–2500 ppm)[4]. While sea surface temperature reconstructions may be biased by local seasonal, latitudinal, and geographical induced variations in temperature[5–7], as well as by preservation issues[8], deep-sea temperature proxy signals are not affected by these processes[9,10]. Deep-sea temperature reconstructions can therefore be used as a reliable indicator of global mean temperatures in the geological past[11,12]. Currently, much of our understanding of global climate evolution and variability during the early Eocene is based on deep-sea temperature estimates derived from benthic foraminiferal oxygen isotopes ($\delta^{18}O$) and Mg/Ca ratios[9,13–16]. For instance, negative excursions in high-resolution stable oxygen and carbon isotope records have revealed the periodical occurrence of multiple transient (10–100 kyr) episodes of global warming and ocean acidification (hyperthermal events; e.g. Paleocene-Eocene

Thermal Maximum, ETM2 and ETM3)[16], likely driven by massive release of isotopically light carbon into the ocean-atmosphere system[1].

Yet, the reliability of foraminiferal $\delta^{18}O$- and Mg/Ca-based temperature reconstructions is hampered by uncertainties in nonthermal factors. Both proxies demand assumptions on the past $\delta^{18}O$ and Mg/Ca composition of the seawater and are influenced by the carbonate chemistry of the ocean and species-specific physiological factors[17–19]. The carbonate clumped isotope proxy (Δ_{47}), which uses the temperature dependence of the bonding of the two heavy rare isotopes (^{13}C and ^{18}O) within the carbonate ion, shows great potential as it is independent of the isotope composition of the seawater and is largely unaffected by pH and biology[20–22]. Recent analytical developments in this technique now allow for analysis of relatively small sample sizes (e.g., foraminifera), and thus enable reconstruction of marine temperatures independent from these non-thermal uncertainties[23–25]. While application of clumped isotope paleothermometry on the relatively cooler Miocene and middle Eocene have revealed a much warmer deep ocean than traditionally accepted[26–28], it is currently not known whether warmer deep-sea temperatures than assumed are also explicit during the hothouse world of the early Eocene.

Here, we report the first Δ_{47}-based deep-sea temperature estimates of the early Eocene and across two hyperthermal events. Early Eocene hyperthermals ETM2 (or H1) and H2 (~54.1 and 54.0 Ma), that occurred approximately 2 Myrs after the PETM, were discovered for the first time in South Atlantic sediment cores[29]. High-resolution (~1 kyr) benthic foraminiferal carbon and oxygen isotope records were generated from four ODP Sites (1262, 1263, 1265 and 1267) at the Walvis Ridge and one site at Maud Rise in the Weddell Sea (ODP Site 690) with paleowater depths ranging from ~1500 m to ~3600 m (ref 30) (Extended Data Fig. 1). The benthic $\delta^{18}O$ records of all these sites show almost identical values, suggesting that they reflect similar deep-sea conditions[30]. Here, we revisit these sites and apply paired stable and clumped isotope analysis on the benthic foraminiferal species *Nuttallides truempyi* and *Oridorsalis umbonatus* for confident reconstruction of deep-sea temperatures across these two hyperthermals.

Stable and clumped isotope analysis

Our new carbon and oxygen isotope measurements (Fig. 1) are consistent with the previously published benthic $\delta^{13}C$ and $\delta^{18}O$ records[30]. Prominent negative excursions in $\delta^{13}C$ (–1.4‰ and –0.8‰, respectively) and $\delta^{18}O$ (–0.8‰ and –0.5‰ respectively) characterize ETM2 and H2, indicating the injection of large amounts of ^{13}C-depleted carbon into the climate system and elevated deep-sea temperatures[29,30]. Limited isotope data is obtained for the peak ETM2 interval at the Walvis Ridge sites, as benthic foraminifera are rare and small-sized in the associated red clay layer, known as the Elmo horizon[29,30].

Due to the sporadic natural abundance of ^{13}C–^{18}O bonds within carbonate ions, clumped isotope analysis is characterized by a low analytical precision[20,23–25]. Averaging multiple replicate Δ_{47} measurements is required to obtain precise estimates of temperature, and therefore demands large sample sizes (>5 mg, each replicate ~100

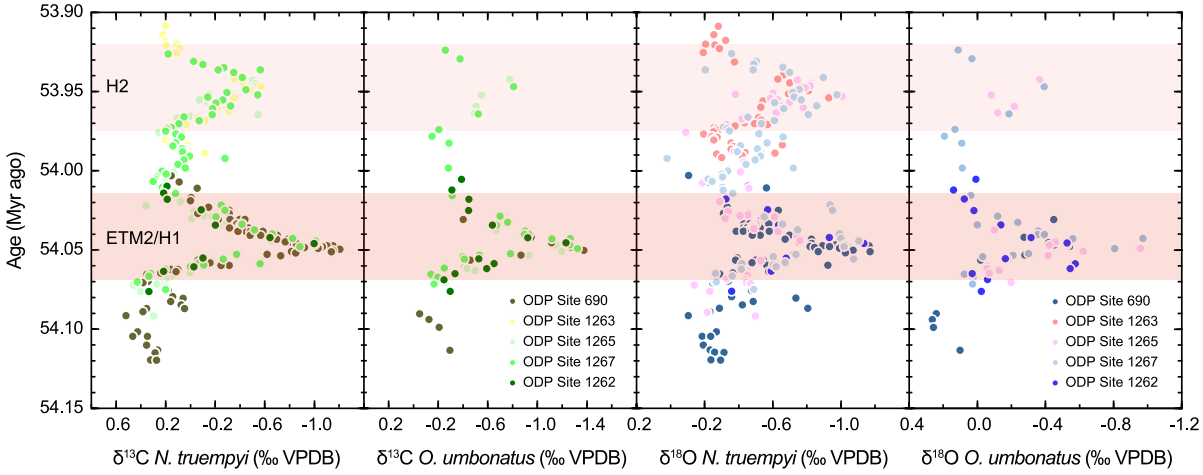

Fig. 1 | South Atlantic benthic foraminiferal $\delta^{13}C$ and $\delta^{18}O$ records across ETM2 and H2. This figure shows the $\delta^{13}C$ and $\delta^{18}O$ measurements for benthic foraminifera *N. truempyi* and *O. umbonatus*. The apparent offset in the stable isotopes between the two species indicates different isotope fractionation[34].

µg)[24,25]. The strategy in how to average Δ_{47} measurements for precise reconstruction of small temperature variability becomes important when sample size is limited[31]. In our study, the abundance of *N. truempyi* and *O. umbonatus* is too low in the samples at all sites to undertake enough measurements for the precise reconstruction of deep-sea temperature change across ETM-2 and H2. As a solution to obtain the desired precision (<3°C at 95% confidence interval), we sorted the Δ_{47} measurements from all sites based on their corresponding $\delta^{18}O$ values and compiled three average clumped isotope temperatures that represent the average background state (high $\delta^{18}O$), average slope (middle $\delta^{18}O$), and average hyperthermal peak (low $\delta^{18}O$) conditions across the studied interval. So instead of showing deep-sea temperatures in a time series, we plotted three clumped isotope temperature bins that are representative for the different climate states. A Welch t-test was performed between the 'high $\delta^{18}O$' and 'low $\delta^{18}O$' Δ_{47} measurements to obtain the most optimal bin size for the background and hyperthermal temperatures[31] (Extended Data Table 1 and Extended Data Figures 2 and 3).

Deep-sea temperatures

Our Δ_{47}-based reconstruction indicates very warm deep waters with average background temperatures of 13.2±1.9 °C (95% CI) and average hyperthermal peak temperatures of 16.5±2.2 °C (95% CI) (Fig. 2b). These temperatures represent an average hyperthermal deep-sea warming of 3.3±2.9 °C (95% CI). The peak temperature of ETM2 cannot be estimated due to the averaging of Δ_{47} data and limited measurements derived from the Elmo horizon. However, the ETM-2 peak temperature may be assumed to be warmer than 16.5±2.2 °C (95% CI) based the magnitude of the stable isotope excursion, being almost twice the magnitude of H2 (ref 30).

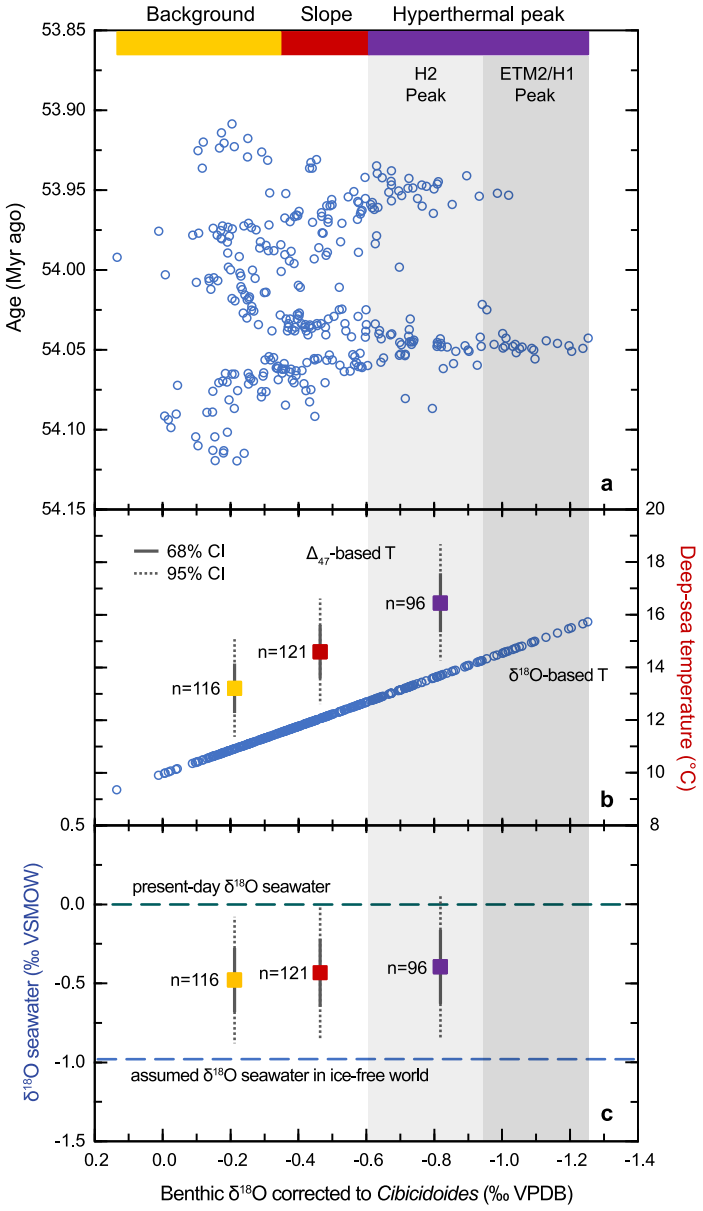

Fig. 2 | Deep-sea temperatures and $\delta^{18}O$ seawater composition. a, Benthic $\delta^{18}O$ values that are corrected towards *Cibicidoides* (for seawater equilibrium) across ETM2 and H2. **b**, Deep-sea temperatures based on benthic Δ_{47} and $\delta^{18}O$ across ETM2 and H2. The yellow, red, and purple (background, slope, hyperthermal peak) bars indicate the range in $\delta^{18}O$ values that correspond to the Δ_{47} measurements used for compiling these three bins. The error bars (68% and 95% CI) in the Δ_{47}-based temperatures represent fully propagated analytical and calibration uncertainties. **c**, $\delta^{18}O_{sw}$ across the ETM2 and H2 interval, which we calculated by using the Δ_{47}-based temperatures in combination with the foraminiferal $\delta^{18}O$ values in the oxygen isotope-temperature relationship of ref 33 (Methods). The uncertainty in the Δ_{47}-based temperatures is propagated to estimate the precision of the $\delta^{18}O_{sw}$ calculations. The dashed red line is the assumed $\delta^{18}O_{sw}$ value based on ice-free conditions, while the dashed blue line represents the present-day icehouse $\delta^{18}O_{sw}$ value.

Our background temperature reconstruction falls within the broad range of possible Mg/Ca-based deep-sea temperatures for the early Eocene, of ~10 to ~15 °C, associated with significant uncertainty in seawater Mg/Ca ratios prior to the middle Eocene[18,32]. Regarding hyperthermal deep-sea temperature change based on Mg/Ca,

reconstructions are currently only available for the PETM and indicate 5–6 °C warming[14]. The deep-sea temperatures we estimate for ETM2 from clumped isotopes suggest that Mg/Ca underestimates deep-sea hyperthermal warming, considering ETM2 has half the magnitude of the PETM based on their stable isotope excursions[16,29,30]. Generally, it is assumed that reconstruction of temperature change across the short-lived hyperthermal events is not influenced by secular (long-term) changes in seawater Mg/Ca composition[18]. Rather, this underestimation of deep-sea temperature variability by Mg/Ca in the Eocene may result from a lowering of the Mg/Ca-temperature sensitivity at low Mg/Ca_{sw} values[19].

To compare the clumped isotope-based deep-sea temperatures with those derived from conventional $\delta^{18}O$, we applied the revised $\delta^{18}O$-temperature relationship of ref 33 on our new data (Methods). As in previous palaeoceanographic research[13], we adopted a fixed value of −0.98‰ VSMOW for the mean oxygen isotopic composition of the seawater ($\delta^{18}O_{sw}$) for the early Eocene global ocean, based on the assumption of absence of continental ice. We adjusted the *N. truempyi* and *O. umbonatus* $\delta^{18}O$ values to *Cibicidoides* using well-documented interspecies offset correction factors for the late Paleocene-early Eocene[34] (Methods). In contrast to previous studies[13,35], we consider no specific offset between the $\delta^{18}O_{sw}$ and the foraminiferal tests of *Cibicidoides*, since recently it has been shown that modern *Cibicidoides* $\delta^{18}O$ values are in close equilibrium with seawater[33]. Note that if we would have applied the generally assumed offset correction of 0.64‰ for this genus[35], our $\delta^{18}O$-based temperature estimates would have been 2−3 °C colder. In comparison to the $\delta^{18}O$-based deep-sea temperatures, our clumped isotope reconstructions are on average two and a half degrees warmer, i.e., 13.2±1.9 °C (95% CI) versus 10.9 °C for background, 14.6±2.0 °C (95% CI) versus 12.1 °C for slope, and 16.5±2.2 °C (95% CI) versus 13.7 °C for average hyperthermal peak temperatures (Fig. 2b).

Constraints on Early Eocene seawater oxygen isotope composition

An important consequence of the warmer Δ_{47}-derived deep-sea temperatures for the early Eocene is that they imply a mean value for $\delta^{18}O_{sw}$ of approximately –0.4±0.4‰ VSMOW (95 % CI), which is much higher than the value of −0.98 ‰ VSMOW based on the assumption of ice-free conditions (Fig. 2c). A first explanation may be that major continental ice sheets were present during the early Eocene. However, this hypothesis can be refuted with subtropical temperatures and vegetation that prevailed at both poles[36,37]. Though small ephemeral ice caps may have been present in Antarctica and in the Arctic region, records of ice rafted debris show that significant high-latitude ice formation was not initiated prior to the middle Eocene[38,39].

In the absence of large ice sheets, a second explanation for our reconstructed higher $\delta^{18}O_{sw}$ value than currently assumed may be that local factors were important for determining the isotopic composition of the deep-water masses in the South Atlantic. As such, the high $\delta^{18}O_{sw}$ value may suggest that saline Atlantic deep waters were more persistent during the early Eocene, perhaps driven by evaporation-dominated deep-water formation at the low-latitudes[40]. However, a complicating factor is that other regions of the deep ocean must have had a much lighter

$\delta^{18}O_{sw}$ (fresher waters) to balance the global ocean $\delta^{18}O_{sw}$ towards ice-free conditions. Such large spatial differences in deep-sea $\delta^{18}O_{sw}$ are difficult to reconcile with small isotope gradients between ocean basins[41].

A third explanation for the high $\delta^{18}O_{sw}$ comes from recent studies that hypothesize that groundwater reservoirs are an important factor in causing the apparent large sea level fluctuations (tens of meters) in hothouse periods during the Cretaceous[42]. Whether such aquifers as large reservoirs for light oxygen on land[42] could explain a high $\delta^{18}O_{sw}$ in the early Eocene hothouse remains an open question.

Potential pH effect on foraminiferal oxygen isotopes and species-specific isotope fractionation

Factors other than a different $\delta^{18}O_{sw}$ may also explain the temperature discrepancy between clumped isotopes and $\delta^{18}O$. The assumed $\delta^{18}O_{sw}$ value of −0.98 ‰ VSMOW may be correct when a pH effect on foraminifera $\delta^{18}O$ is taking into account. A much lower deep-sea pH existed during the early Eocene (~0.4 units lower than modern)[43]. Both culture experiments and field studies have shown that foraminiferal $\delta^{18}O$ is sensitive to pH, characterized by increasing $\delta^{18}O$ values with decreasing pH, but with a varying magnitude of this effect among different species[44]. Although this pH effect on $\delta^{18}O$ has so far not been demonstrated for benthic foraminifera[33], the underestimated early Eocene deep-sea temperatures indicated by $\delta^{18}O$ are consistent with a scenario of highly reduced sea water pH. Though actual proxy deep-sea pH reconstructions are currently not available for the hyperthermals, a further acidification of the deep water is expected from numerical models[45]. The assumed effect of an even lower pH would result in a dampening of the negative benthic foraminiferal $\delta^{18}O$ excursion of these warming events (almost half of the original magnitude)[45], with a consequent underestimation of the deep-sea warming. Based on our proxy reconstruction, it is though not possible to support that $\delta^{18}O$ underestimates hyperthermal deep-sea warming with one degree Celsius or more due to the temperature uncertainty in the clumped isotope bins and the maximum hyperthermal peak temperatures that cannot be estimated due the averaging approach.

In addition to a potential pH effect, changes in species-specific isotope fractionation over time are also important to consider as a possible explanation for the relatively cold $\delta^{18}O$-based deep-sea temperatures. Whether modern foraminiferal species precipitate their calcite tests with a certain offset from seawater has been determined from culture experiments and core top studes[33,35]. Yet, differences in interspecies offsets in $\delta^{18}O$ (and $\delta^{13}C$) have been found between the Paleogene and more recent times[34]. These different offsets may suggest that vital effects were not constant through the Cenozoic, which are however difficult to quantify[34], considering the evolutionary and pH changes that may have played a role through time. In conclusion, our study shows that all these uncertainties in the conventional proxies hamper confident deep-sea temperature reconstructions of the Eocene. The reliability of these classic reconstructions can also be questioned for other periods of the Cenozoic, such as the Miocene[26,27]. These findings clearly warrant a revision of the traditional Cenozoic history of deep-sea temperatures that has provided us with a presumed benchmark of our understanding of global climate evolution over the past 66 Myrs[13,15].

Implications for climate sensitivity in the early Eocene

To incorporate our new constraints on early Eocene deep-sea temperatures based on clumped isotopes in a broader perspective of the Eocene climate state, we assume that the reconstructed South Atlantic deep-sea temperatures are representative for the global deep sea, i.e., a homogeneous global deep ocean. This assumption of globally uniform deep-sea temperatures is supported by the small interbasinal isotopic differences found for the early Paleogene[41], and almost identical clumped isotope-based deep-sea temperatures across the Atlantic for middle Eocene times[28]. As such, our new constraints on deep-sea temperatures have important implications for estimates for Equilibrium Climate Sensitivity (ECS), defined as the equilibrium global mean temperature (GMT) increase in response to a doubling in atmospheric CO_2 (ref 11), of the early Eocene.

In order to estimate ECS from our data, we need to transfer deep-sea temperatures to GMT estimates. Following previous studies[46,47], we apply the assumption that in warmer climates prior to the Pliocene deep-sea temperature change scales directly to GMT change ($\Delta GMT = \Delta DT$) (ref 12). In the icehouse climate state of the Pleistocene, this relation may be different and therefore deep-sea temperature change could be smaller than the GMT change[12] (Methods). Using this approach with a $\delta^{18}O$-based Pliocene deep-sea temperature of 2 °C (ref 12) based on the assumption of a 2:1 contribution of temperature and ice volume respectively on benthic $\delta^{18}O$ (Methods), we derive a GMT of 28.4±1.9 °C (95% CI) for background early Eocene conditions from our reconstructed deep-sea temperatures. We note that all the assumptions made here introduce uncertainty in the GMT and consequently ECS estimates. Future independent deep-sea temperature reconstructions from clumped isotopes for the entire Cenozoic will provide more constraints on these scaling factors.

To characterize radiative forcing, we use the recently published CO_2 level reconstructions for the Eocene at 54 Ma from ref 4, showing background CO_2 levels of 900±200 ppmv (95% CI), i.e., >3 times preindustrial (278 ppmv) values. We do not assess ECS during peak conditions of ETM2 (~5 degrees global warming), as the magnitude of the carbon cycle perturbation of this event is not well-constrained yet[48]. To isolate the GMT change purely ascribed to a change in CO_2 forcing, an important step beforehand is to account for the different boundary conditions of the early Eocene, such as the absence of global ice sheets and a different continental configuration. Climate model comparison of the Eocene and preindustrial worlds, both simulated with preindustrial CO_2 forcing, shows that GMT are 3−5 degrees warmer in the Eocene case[49]. Therefore, to correct for the different boundary conditions we subtract this 3−5 degrees temperature range from the GMT difference between the early Eocene and preindustrial. Employing the equations used by ref 4 (Methods), we then obtain an early Eocene ECS of 5.9 °C (3.6 to 9.8 °C 95% CI) per doubling of CO_2. This estimate is close to ECS inferred by recent climate models for the Eocene in which processes like cloud feedbacks operating in much warmer worlds appear to play a key role in amplifying CO_2-induced warmth[50]. Our new deep-sea temperature reconstructions of the early Eocene provide new evidence for high ECS in hothouse climates, supporting a climate state dependency of ECS[4,50]. Such state dependency of ECS

208 may have major implications for the IPCC projections of future warming, as these currently follow the typically
209 estimated range in present-day ECS (1.5 to 4.5 °C).
210
211 **References**

212 1. Zachos, J. C., Dickens, G. R. & Zeebe, R. E. An early Cenozoic perspective on greenhouse warming and
213 carbon-cycle dynamics. *Nature* **451**, 279–283 (2008).
214 2. Burke, K. D. *et al*. Pliocene and Eocene provide best analogs for near-future climates. *Proceedings of the*
215 *National Academy of Sciences* **115**, 13288-13293 (2018).
216 3. Cramwinckel, M. J. *et al*. Synchronous tropical and polar temperature evolution in the Eocene. *Nature* **559**,
217 382-386 (2018).
218 4. Anagnostou, E. *et al*. Proxy evidence for state-dependence of climate sensitivity in the Eocene greenhouse.
219 *Nature communications* **11**, 1–9 (2020).
220 5. Hollis, C. J. *et al*. Early Paleogene temperature history of the Southwest Pacific Ocean: Reconciling proxies
221 and models. *Earth Planet. Sci. Lett.* **349**, 53-66 (2012).
222 6. Davies, A., Hunter, S. J., Gréselle, B., Haywood, A. M. & Robson, C. Evidence for seasonality in early
223 Eocene high latitude sea-surface temperatures. *Earth Planet. Sci. Lett.* **519**, 274-283 (2019).
224 7. Judd, E. J., Bhattacharya, T. & Ivany, L. C. A dynamical framework for interpreting ancient sea surface
225 temperatures. *Geophys. Res. Lett.* **47**, e2020GL089044 (2020).
226 8. Pearson, P. N. & Burgess, C. E. Foraminifer test preservation and diagenesis: comparison of high latitude
227 Eocene sites. *Geological Society, London, Special Publications* **303**, 59-72 (2008).
228 9. Lear, C. H., Elderfield, H. & Wilson, P. A. Cenozoic deep-sea temperatures and global ice volumes from
229 Mg/Ca in benthic foraminiferal calcite. *Science* **287**, 269-272 (2000).
230 10. Voigt, J., Hathorne, E. C., Frank, M. & Holbourn, A. Minimal influence of recrystallization on middle Miocene
231 benthic foraminiferal stable isotope stratigraphy in the eastern equatorial Pacific. *Paleoceanography* **31**, 98–
232 114 (2016).
233 11. PALAEOSENS Project Members. Making sense of palaeoclimate sensitivity. *Nature* **491**, 683–691 (2012).
234 12. Hansen, J., Sato, M., Russell, G. & Kharecha, P. Climate sensitivity, sea level and atmospheric carbon
235 dioxide. *Philosophical Transactions of the Royal Society A: Mathematical, Physical and Engineering*
236 *Sciences* **371**, 20120294 (2013).
237 13. Zachos, J., Pagani, M., Sloan, L., Thomas, E. & Billups, K. Trends, rhythms, and aberrations in global climate
238 65 Ma to present. *Science* **292**, 686–693 (2001).
239 14. Tripati, A. & Elderfield, H. Deep-sea temperature and circulation changes at the Paleocene-Eocene thermal
240 maximum. *Science* **308**, 1894–1898 (2005).

15. Cramer, B. S., Miller, K. G., Barrett, P. J. & Wright, J. D. Late Cretaceous–Neogene trends in deep ocean temperature and continental ice volume: Reconciling records of benthic foraminiferal geochemistry (δ18O and Mg/Ca) with sea level history. *Journal of Geophysical Research: Oceans* **116,** (2011).
16. Lauretano, V., Zachos, J. C. & Lourens, L. J. Orbitally paced carbon and deep-sea temperature changes at the peak of the early Eocene climatic optimum. *Paleoceanography and Paleoclimatology* **33**, 1050–1065 (2018).
17. Pearson, P. N. Oxygen isotopes in foraminifera: Overview and historical review. *The Paleontological Society Papers* **18**, 1–38 (2012).
18. Evans, D. & Müller, W. Deep time foraminifera Mg/Ca paleothermometry: Nonlinear correction for secular change in seawater Mg/Ca. *Paleoceanography* **27** (2012).
19. Evans, D., Wade, B. S., Henehan, M., Erez, J. & Müller, W. Revisiting carbonate chemistry controls on planktic foraminifera Mg/Ca: implications for sea surface temperature and hydrology shifts over the Paleocene–Eocene Thermal Maximum and Eocene–Oligocene transition. *Climate of the Past* **12**, 819-835 (2016).
20. Eiler, J. M. Paleoclimate reconstruction using carbonate clumped isotope thermometry. *Quaternary Science Reviews* **30**, 3575-3588 (2011).
21. Tripati, A. K. *et al*. Beyond temperature: Clumped isotope signatures in dissolved inorganic carbon species and the influence of solution chemistry on carbonate mineral composition. *Geochim. Cosmochim. Acta* **166**, 344-371 (2015).
22. Peral, M. *et al*. Updated calibration of the clumped isotope thermometer in planktonic and benthic foraminifera. *Geochim. Cosmochim. Acta* **239**, 1–16 (2018).
23. Meckler, A. N., Ziegler, M., Millán, M. I., Breitenbach, S. F. & Bernasconi, S. M. Long-term performance of the Kiel carbonate device with a new correction scheme for clumped isotope measurements. *Rapid Communications in Mass Spectrometry* **28**, 1705–1715 (2014).
24. Müller, I. A. *et al*. Carbonate clumped isotope analyses with the long-integration dual-inlet (LIDI) workflow: Scratching at the lower sample weight boundaries. *Rapid Communications in Mass Spectrometry* **31**, 1057–1066 (2017).
25. Bernasconi, S. M. *et al*. Reducing uncertainties in carbonate clumped isotope analysis through consistent carbonate-based standardization. *Geochem. Geophys. Geosyst.* **19**, 2895–2914 (2018).
26. Modestou, S. E., Leutert, T. J., Fernandez, A., Lear, C. H. & Meckler, A. N. Warm middle Miocene Indian Ocean bottom water temperatures: Comparison of clumped isotope and Mg/Ca-based estimates. *Paleoceanography and Paleoclimatology* **35**, e2020PA003927 (2020).
27. Evans, D. Deep heat: proxies, Miocene ice, and an end in sight for paleoclimate paradoxes? *Paleoceanography and Paleoclimatology* **36**, e2020PA004174 (2021).

28. Leutert, T. J. *et al*. Sensitivity of clumped isotope temperatures in fossil benthic and planktic foraminifera to diagenetic alteration. *Geochim. Cosmochim. Acta* **257**, 354–372 (2019).
29. Lourens, L. J. *et al*. Astronomical pacing of late Palaeocene to early Eocene global warming events. *Nature* **435**, 1083–1087 (2005).
30. Stap, L. *et al*. High-resolution deep-sea carbon and oxygen isotope records of Eocene Thermal Maximum 2 and H2. *Geology* **38**, 607–610 (2010).
31. de Winter, N., Agterhuis, T. & Ziegler, M. Optimizing sampling strategies in high-resolution paleoclimate records. *Climate of the Past Discussions*, 1-52 (2020).
32. Miller, K. G. *et al*. Cenozoic sea-level and cryospheric evolution from deep-sea geochemical and continental margin records. *Science advances* **6**, eaaz1346 (2020).
33. Marchitto, T. M. *et al*. Improved oxygen isotope temperature calibrations for cosmopolitan benthic foraminifera. *Geochim. Cosmochim. Acta* **130**, 1–11 (2014).
34. Katz, M. E. *et al*. Early Cenozoic benthic foraminiferal isotopes: Species reliability and interspecies correction factors. *Paleoceanography* **18,** (2003).
35. Shackleton, N. J. Attainment of isotopic equilibrium between ocean water and the benthonic foraminifera genus Uvigerina: Isotopic changes in the ocean during the last glacial. *Colloq. Int. C. N. R. S.* **219**, 203–209 (1974).
36. Pross, J. *et al*. Persistent near-tropical warmth on the Antarctic continent during the early Eocene epoch. *Nature* **488**, 73-77 (2012).
37. Willard, D. A. *et al*. Arctic vegetation, temperature, and hydrology during Early Eocene transient global warming events. *Global Planet. Change* **178**, 139-152 (2019).
38. Tripati, A., Backman, J., Elderfield, H. & Ferretti, P. Eocene bipolar glaciation associated with global carbon cycle changes. *Nature* **436**, 341-346 (2005).
39. Stickley, C. E. *et al*. Evidence for middle Eocene Arctic sea ice from diatoms and ice-rafted debris. *Nature* **460**, 376-379 (2009).
40. Lunt, D. J. *et al*. CO2-driven ocean circulation changes as an amplifier of Paleocene-Eocene thermal maximum hydrate destabilization. *Geology* **38**, 875–878 (2010).
41. Cramer, B. S., Toggweiler, J. R., Wright, J. D., Katz, M. E. & Miller, K. G. Ocean overturning since the Late Cretaceous: Inferences from a new benthic foraminiferal isotope compilation. *Paleoceanography* **24,** (2009).
42. Sames, B., Wagreich, M., Conrad, C. P. & Iqbal, S. Aquifer-eustasy as the main driver of short-term sea-level fluctuations during Cretaceous hothouse climate phases. *Geological Society, London, Special Publications* **498**, 9-38 (2020).
43. Raitzsch, M. & Hönisch, B. Cenozoic boron isotope variations in benthic foraminifers. *Geology* **41**, 591-594 (2013).

44. Spero, H. J., Bijma, J., Lea, D. W. & Bemis, B. E. Effect of seawater carbonate concentration on foraminiferal carbon and oxygen isotopes. *Nature* **390**, 497–500 (1997).
45. Uchikawa, J. & Zeebe, R. E. Examining possible effects of seawater pH decline on foraminiferal stable isotopes during the Paleocene-Eocene Thermal Maximum. *Paleoceanography* **25,** (2010).
46. Inglis, G. N. *et al*. Global mean surface temperature and climate sensitivity of the early Eocene Climatic Optimum (EECO), Paleocene–Eocene Thermal Maximum (PETM), and latest Paleocene. *Climate of the Past* **16**, 1953-1968 (2020).
47. Westerhold, T. *et al*. An astronomically dated record of Earth's climate and its predictability over the last 66 million years. *Science* **369**, 1383-1387 (2020).
48. Harper, D. T. *et al*. The magnitude of surface ocean acidification and carbon release during Eocene Thermal Maximum 2 (ETM-2) and the Paleocene-Eocene Thermal Maximum (PETM). *Paleoceanography and Paleoclimatology* **35**, e2019PA003699 (2020).
49. Lunt, D. J. *et al*. DeepMIP: Model intercomparison of early Eocene climatic optimum (EECO) large-scale climate features and comparison with proxy data. *Climate of the Past* **17**, 203-227 (2021).
50. Zhu, J., Poulsen, C. J. & Tierney, J. E. Simulation of Eocene extreme warmth and high climate sensitivity through cloud feedbacks. *Science Advances* **5**, eaax1874 (2019).

Acknowledgements This research was conducted under the program of the Netherlands Earth System Science Centre (NESSC), financially supported by the Ministry of Education, Culture and Sciences (OCW) of the Netherlands. This work used samples and data provided by the Ocean Drilling Program (ODP). We thank I.J. Kocken (Utrecht University) for processing the clumped isotope data archive with his R script, and A. E. van Dijk (Utrecht Geolab) for technical support in the lab.

Author contributions T.A., M.Z., and L.J.L. designed the study. T.A. generated the stable and clumped isotope data. All authors contributed to data interpretation and the written manuscript.

Competing interests The authors declare no competing interests.

Materials and correspondence requests should be addressed to T.A.

METHODS

Foraminiferal preservation and sampling. Since recently, clumped isotope thermometry has been applied on foraminifera in several paleoclimate studies[26,28,51–54]. In our study to the early Eocene, we performed stable and clumped isotope measurements on monospecific multispecimen samples of *Nuttallides truempyi* and *Oridorsalis*

umbonatus, which were picked from the >212 µm sediment size fractions of the samples of the previous study of ref 30. Grouping of Δ_{47} measurements from different benthic species together to produce one temperature estimate requires the assumption of absence of species-specific effects on Δ_{47}. This assumption is supported by both modern core top and deep time studies that show no indication of these biological factors[22,26,51,55–58]. Scanning electron microscope (SEM) images were previously generated to examine the preservation throughout the studied interval and indicate that the foraminiferal tests are moderately altered by recrystallization/secondary calcite[30]. Nevertheless, the effect of recrystallization of primary calcite on the Δ_{47} signal in benthic foraminifera has been shown to be largely negligible[26,28,59], since this diagenesis usually occurs during early burial[10,60,61], and therefore records similar temperatures as the seafloor temperatures. Due to limiting numbers of picked foraminifera per sample, we needed to combine picked foraminifers of neighboring depths to enable sufficient foraminiferal material (~25 specimens per measurement). Prior to isotope analysis, foraminiferal samples were cleaned by removing adherent contaminants, for instance nannofossils, organics and clay particles. The foraminifers were gently cracked between two glass plates to enable any chamber infill to escape, and subsequently sonicated in deionized water two times for 20 seconds. The test fragments were rinsed until the suspended particles were removed (~2 x 2 times), and oven-dried at 40 °C for one night.

Clumped isotope analysis. In total, 333 successful stable and clumped isotope sample measurements were generated across the ETM2 and H2 interval. Our analytical methods generally follow previous work[23,24], and a more detailed description can be found in the Supplementary Information. We performed measurements of ~100 µg foraminiferal material each on a *Thermo Scientific Kiel IV* carbonate preparation device coupled to a *Thermo Scientific MAT 253 Plus* mass spectrometer at Utrecht University. Apart from samples, we measured additional carbonate standards in an approximate 1:1 ratio. We employed three standards (ETH-1, 2, and 3), which differ in $\delta^{13}C$, $\delta^{18}O$, and Δ_{47} composition, to correct the results and monitor the long-term reproducibility. Two additional check standards (IAEA-C2 and Merck) were also measured to evaluate this long-term instrument performance. External reproducibility (one standard deviation) in Δ_{47} of all the carbonate standards after correction was typically 0.030–0.040‰. The $\delta^{13}C$ and $\delta^{18}O$ values (reported relative to the VPDB scale) of the standards show an external reproducibility (one standard deviation) of respectively 0.10 and 0.05‰ on average. In Fig. 1, the stable isotope data is plotted against age following the age models of refs 30,62.

Temperature calculations. To determine clumped isotope-based deep-sea temperatures, we employed a recent foraminifer-based calibration[58] recalculated to the Intercarb-Carbon Dioxide Equilibrium Scale (I-CDES) using the newly accepted values of the carbonate standards of ref 63.

$$\Delta_{47}(I\text{–}CDES 90°C) = 0.0407(\pm 0.0016) \cdot 10^6/T^2 + 0.1385\ (\pm 0.0189)\ (T \text{ in K}) \quad (1)$$

This Δ_{47}-temperature relationship represents a composite of previously published foraminifer based-calibrations[22,57] with new data[58]. Within uncertainty, this regression is consistent with calibrations based on inorganic calcite[25,64]. For our data representation and visualization, we fully propagated analytical and calibration uncertainties in the temperature estimates. The combined uncertainty is reported as 68% and 95% confidence intervals (CI) in the temperature bins.

Calculation of the $\delta^{18}O$-based deep-sea temperatures follows equation 9 of ref 33 based on the benthic foraminifera *Cibicidoides*:

$$\delta^{18}O_b\ [‰\ VPDB] - \delta^{18}O_{sw}\ [‰\ VSMOW] + 0.27 = -0.245T + 0.0011T^2 + 3.58 \quad (2)$$

This quadratic regression shows good agreement with the calibration of ref 65, which is based on inorganic calcite precipitated between 10 and 40 °C[65,66]. Prior to temperature calculation, we adjusted $\delta^{18}O$ of *O. umbonatus* and *N. truempyi* towards *Cibicoides* values for assumed seawater equilibrium using the following correction factors from ref 34: (Nutt + 0.10)/0.89 = Cib; and Orid − 0.28 = Cib.

Global mean temperatures. Previous studies have used $\delta^{18}O$-based deep-sea temperature to estimate GMT[11,12,46,47]. We calculated GMT from our reconstructed Δ_{47}-based deep-sea temperatures following the rationale of ref 12,67,68, who suggest that deep-sea temperature change is similar to GMT change when several degrees above the freezing point of ocean water. This approach argues that deep-sea temperatures are closely related to high-latitude (region of deep-water formation) sea surface temperatures, and changes in the latter are amplified relative to the global mean sea surface temperature change. Yet, the air temperature change on the continents is larger than in the mean surface ocean. Ref 12,67,68 suggest that these two factors are offsetting in relatively equal proportions, and therefore they assume that temperature change in the deep-ocean tends to approximate the GMT change. They use surface temperature reconstructions and climate model results for the Eocene, the Pliocene, and the Last Glacial Maximum to determine the exact relationship between deep-sea temperature and GMT change during different periods in Cenozoic. Deep-sea temperature change is proposed to be tied to GMT change in a 1:1 ratio for the pre-Pliocene (ΔGMT = ΔDT), though they do not disregard the possibility of a ΔGMT = 1.5 x ΔDT relationship, which shows more consistency with sea surface temperature reconstructions (which in the higher latitudes though may be overestimated due to a potential summer bias)[12]. In the Late Cenozoic Pliocene and Pleistocene, however, this scaling changes, as the deep ocean cannot become much colder when it approaches the freezing temperature of ocean water. In other words, in these cooler climates the deep-sea temperature change is smaller than the GMT change[12,67,68]. Combining the pre-Pliocene relationship (ΔGMT = ΔDT) and the Pliocene relationship (equation 4.2 in ref. 12) results in the following equation to calculate GMT of the early Eocene:

$$\mathbf{GMT_{Eocene}\ (°C)} = (2.5 \times DST_{Plio} + 12.15)\ \mathbf{[=GMT_{Plio}]} + (DST_{Eocene} - DST_{Plio}) \quad (3)$$

where we use a Pliocene and early Eocene deep-sea temperature of respectively 2 °C (ref 12) and 13.2±1.9 °C. This Pliocene deep-sea temperature of 2 °C is based on benthic $\delta^{18}O$ assuming a 2:1 contribution of temperature and ice volume respectively from sea level reconstructions[12].

Climate sensitivity. To determine ECS, we follow the approach in refs 4,46,69. We first calculate the relative change in climate forcing (Wm^{-2}) attributed to a CO_2 change in the early Eocene relative to preindustrial using the equation of ref 70:

$$\Delta F_{CO2} = 5.32\ln(C_{EE}/C_{PI}) + 0.39[\ln(C_{EE}/C_{PI})]^2 \quad (4)$$

where C_{EE} represents the background atmospheric CO_2 levels in the early Eocene (at 54 Ma), and C_{PI} refers to the CO_2 concentrations during the preindustrial (278 ppm).

ECS of the early Eocene relative to preindustrial is obtained using the following equation[4,46,69]:

$$ECS = (\Delta GMT_{EE\text{-}vs\text{-}PI}/\Delta F_{CO2}) \times 3.87 \quad (5)$$

where $\Delta GMT_{EE\text{-}vs\text{-}PI}$ is the GMT change that is attributed to a change in CO_2 forcing, and $\Delta F_{CO2\text{-}vs\text{-}PI}$ indicates the relative change in climate forcing by CO_2. The 3.87 (in Wm^{-2}) expresses the climate forcing of a doubling in CO_2.

We account for the contribution of different paleogeography and paleotopography, solar constant, and slow climate feedbacks associated with ice sheets (absence), vegetation, and aerosols to the GMT difference between early Eocene and preindustrial (GMT of 28.4±1.9 °C and 14 °C for the early Eocene and preindustrial respectively). Based on climate model simulations[49], we subtract a value of 3−5 degrees from the early Eocene GMT to obtain the temperature change that is purely ascribed to different CO_2 forcing.

References

51. Thornalley, D. J. *et al*. A warm and poorly ventilated deep Arctic Mediterranean during the last glacial period. *Science* **349**, 706-710 (2015).
52. Rodríguez-Sanz, L. *et al*. Penultimate deglacial warming across the Mediterranean Sea revealed by clumped isotopes in foraminifera. *Scientific Reports* **7**, 1–11 (2017).
53. Leutert, T. J., Auderset, A., Martínez-García, A., Modestou, S. & Meckler, A. N. Coupled Southern Ocean cooling and Antarctic ice sheet expansion during the middle Miocene. *Nature Geoscience* **13**, 634–639 (2020).
54. Leutert, T. J., Modestou, S., Bernasconi, S. M. & Meckler, A. N. Southern Ocean bottom water cooling and ice sheet expansion during the middle Miocene climate transition. *Climate of the Past Discussions*, 1–26 (2020).

55. Tripati, A. K. *et al*. 13C–18O isotope signatures and 'clumped isotope'thermometry in foraminifera and coccoliths. *Geochim. Cosmochim. Acta* **74**, 5697–5717 (2010).
56. Grauel, A. *et al*. Calibration and application of the 'clumped isotope'thermometer to foraminifera for high-resolution climate reconstructions. *Geochim. Cosmochim. Acta* **108**, 125–140 (2013).
57. Piasecki, A. *et al*. Application of clumped isotope thermometry to benthic foraminifera. *Geochem. Geophys. Geosyst.* **20**, 2082–2090 (2019).
58. Meinicke, N. *et al*. A robust calibration of the clumped isotopes to temperature relationship for foraminifers. *Geochim. Cosmochim. Acta* **270**, 160–183 (2020).
59. Stolper, D. A., Eiler, J. M. & Higgins, J. A. Modeling the effects of diagenesis on carbonate clumped-isotope values in deep-and shallow-water settings. *Geochim. Cosmochim. Acta* **227**, 264–291 (2018).
60. Edgar, K. M., Pälike, H. & Wilson, P. A. Testing the impact of diagenesis on the δ18O and δ13C of benthic foraminiferal calcite from a sediment burial depth transect in the equatorial Pacific. *Paleoceanography* **28**, 468–480 (2013).
61. Voigt, J., Hathorne, E. C., Frank, M., Vollstaedt, H. & Eisenhauer, A. Variability of carbonate diagenesis in equatorial Pacific sediments deduced from radiogenic and stable Sr isotopes. *Geochim. Cosmochim. Acta* **148**, 360–377 (2015).
62. Westerhold, T. *et al*. Astronomical calibration of the Ypresian timescale: implications for seafloor spreading rates and the chaotic behavior of the solar system? *Climate of the Past* **13,** (2017).
63. Bernasconi, S. M., Daëron, M., Bergmann, K. D., Bonifacie, M. & Meckler, A. N. A community effort to improve inter-laboratory standardization of the carbonate clumped isotope thermometer using carbonate anchors. *Earth and Space Science Open Archive ESSOAr* (2020).
64. Kele, S. *et al*. Temperature dependence of oxygen-and clumped isotope fractionation in carbonates: a study of travertines and tufas in the 6–95 C temperature range. *Geochim. Cosmochim. Acta* **168**, 172-192 (2015).
65. Kim, S. & O'Neil, J. R. Equilibrium and nonequilibrium oxygen isotope effects in synthetic carbonates. *Geochim. Cosmochim. Acta* **61**, 3461–3475 (1997).
66. Bemis, B. E., Spero, H. J., Bijma, J. & Lea, D. W. Reevaluation of the oxygen isotopic composition of planktonic foraminifera: Experimental results and revised paleotemperature equations. *Paleoceanography* **13**, 150–160 (1998).
67. Hansen, J. *et al*. Target atmospheric CO2: Where should humanity aim? *arXiv preprint arXiv:0804.1126* (2008).
68. Hansen, J. E. & Sato, M. in *Climate change* 21-47 (Springer, 2012).
69. Anagnostou, E. *et al*. Changing atmospheric CO_2 concentration was the primary driver of early Cenozoic climate. *Nature* **533**, 380-384 (2016).
70. Byrne, B. & Goldblatt, C. Radiative forcing at high concentrations of well-mixed greenhouse gases. *Geophys. Res. Lett.* **41**, 152–160 (2014).

71. Zachos, J. C. *et al*. Rapid acidification of the ocean during the Paleocene-Eocene thermal maximum. *Science* **308**, 1611–1615 (2005).

72. Kennett, J. P. & Stott, L. D. Abrupt deep-sea warming, palaeoceanographic changes and benthic extinctions at the end of the Palaeocene. *Nature* **353**, 225–229 (1991).

Extended data

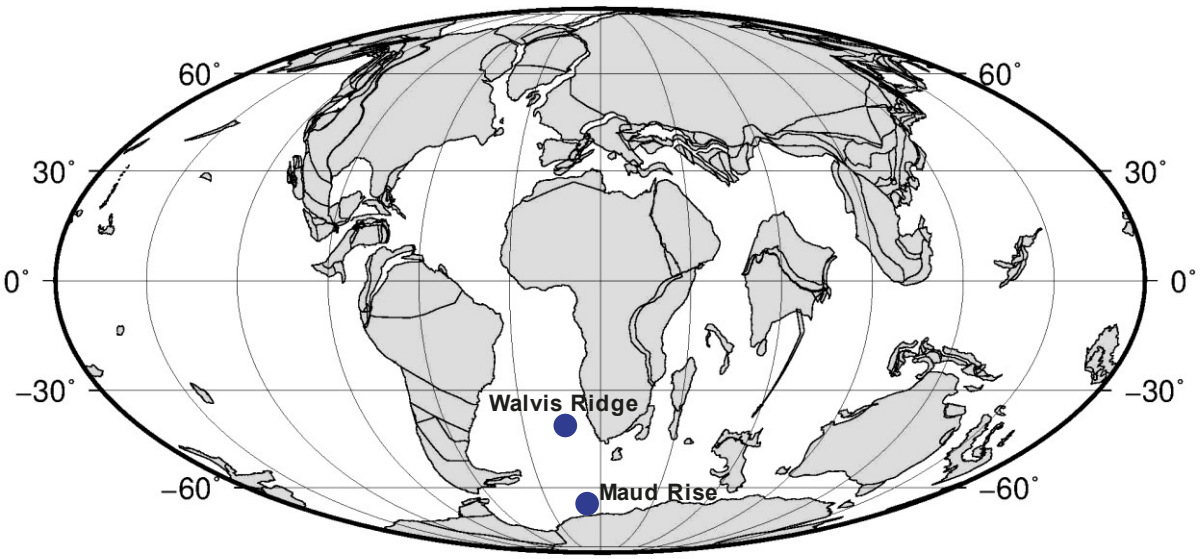

Extended Data Fig. 1 | Paleogeographic reconstruction (54.0 Ma) with location of Walvis Ridge and Maud Rise. This map is generated from the plate tectonic reconstruction service of the Ocean Drilling Stratigraphic Network (ODSN; http://www.odsn.de). The ODP Sites from the Walvis Ridge used for benthic foraminiferal stable and clumped isotope analysis include Sites 1262, 1263, 1265 and 1267. Paleowater depth ranges from ~1500 m (Site 1263) to ~3600 m (Site 1262)[71]. Maud Rise is represented by ODP Site 690 with a paleowater depth of ~2100 m)[72].

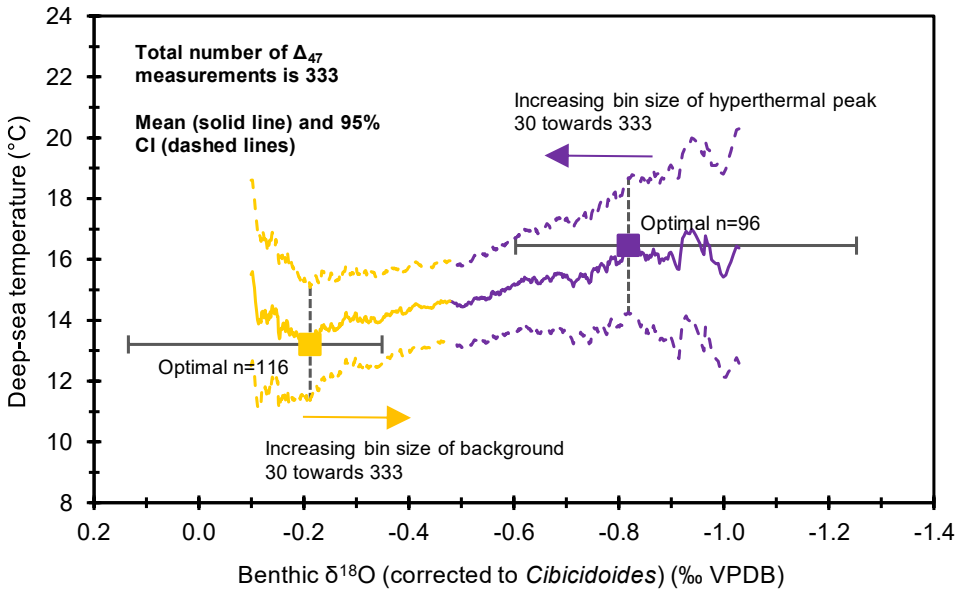

Extended Data Fig. 2 | Background and hyperthermal peak temperatures (mean and 95% CI) as a function of bin size. Adding Δ_{47} measurements with progressively lower and higher $\delta^{18}O$ values results in increasing bin sizes of the background (orange) and hyperthermal peak (purple) states respectively. The mean values of these two bins move towards each other with increasing bin size. The 95% CI decreases with increasing bin size. A size of 116 and 96 Δ_{47} measurements for the background and hyperthermal peak bins respectively yields the most significant difference between the two populations.

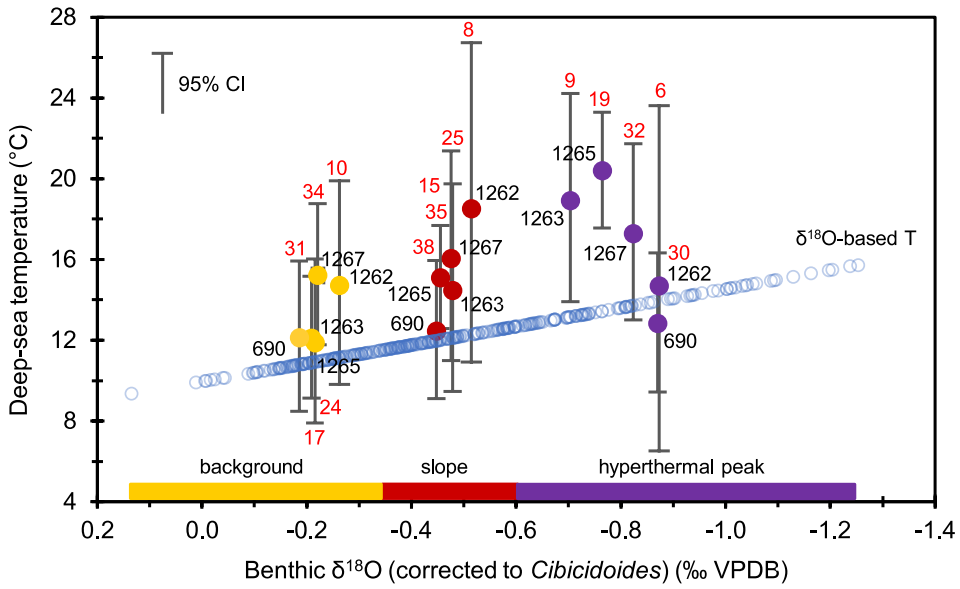

Extended Data Fig. 3 | The compiled Δ_{47}-based temperature bins (background, slope and hyperthermal peak) deconvolved into data per site (mean and 95% CI). The variability in the temperatures among the sites can attributed to limited measurements. Deep-sea temperatures at Site 690 though seem to be slightly cooler in comparison to the Walvis Ridge sites. However, it is not possible to state this with confidence due to the uncertainty in the temperature estimates.

Extended Data Table 1 | Optimal Δ_{47} bin sizes. Overview of the 30 most optimal bin sizes for the background and hyperthermal peak Δ_{47} populations determined using a Welch t-test, i.e., the bin sizes that result in the most significant difference (lowest p-values).

Δ_{47} bin size background	Δ_{47} bin size hyperthermal peak	Lowest p-values
116	96	0.0191
116	93	0.0199
116	97	0.0204
116	94	0.0204
116	99	0.0214
111	96	0.0215
116	92	0.0216
116	95	0.0218
111	93	0.0223
118	96	0.0229
111	94	0.0229
111	97	0.0230
116	98	0.0230
117	96	0.0237
118	93	0.0238
111	99	0.0241
111	92	0.0242
116	100	0.0243
116	91	0.0243
118	94	0.0244
118	97	0.0244
111	95	0.0244
119	96	0.0245
117	93	0.0246
115	96	0.0247
116	55	0.0249
117	94	0.0253
117	97	0.0253
119	93	0.0254
120	96	0.0255

Supplementary Information

Mass spectrometry and clumped isotope data processing

In total, we carried out 27 runs with most of them containing 20 samples interspersed with 26 carbonate standards, over a period of one year. We randomized the distribution of the samples over this period to prevent biases in the obtained data due to variability and longer-term trends in the mass spectrometer performance. The relative

519 proportions of the measured standards ETH-1:ETH-2:ETH-3 was 1:1:10, as optimal minimization of uncertainties
520 in the Δ_{47} data is achieved by measuring relatively more ETH-3 (ref 73). In the *Thermo Scientific Kiel IV* device, the
521 carbonate material was digested with phosphoric acid (H_3PO_4) at a reaction temperature of 70 °C (ref 74). Steps
522 were subsequently taken in the instrument to purify the sample gas. First, the gas was transported to a first
523 cryogenic liquid nitrogen (LN_2) trap with a temperature of –196 °C. Here, CO_2 and H_2O amongst others were frozen
524 and trapped while non-condensable gases (originating from impurities in the sample) were removed[74]. The gas was
525 then transferred through a Porapak-Q trap cooled at –40 °C to remove organic contaminants, such as halo-
526 /hydrocarbons and reduced sulfur compounds[74]. After a second cold trap a near pure CO_2 gas remained, which
527 was sent into the *Thermo Scientific MAT 253 Plus* instrument for isotope analysis. The mass spectrometer collected
528 the signals of m/z 44–49 of the gas, which correspond with the different isotopologues of CO_2 (refs 74, 75). The m/z
529 48 and 49 signals were used to detect potential contamination[76]. To obtain the necessary accuracy of the
530 measurements, the sample gas was measured against a reference gas of known isotopic composition[24,77].
531 Measurements with the mass spectrometer followed the long-integration dual-inlet (LIDI) method[24,78].
532 We applied a pressure sensitive baseline correction (PBL) to correct the obtained data for negative backgrounds
533 using peak scans at m/z 44 intensities of 5, 10, 15, 20, and 25 V, which were performed during run preparation[23,76,79].
534 Subsequently, the ETH-1, ETH-2, and ETH-3 standards were used to correct sample Δ_{47} data and normalize it into
535 the InterCarp-Carbon Dioxide Equilibrium Scale (I-CDES)[25,63,80], to correct for offsets in $\delta^{13}C$ and $\delta^{18}O$, and to
536 correct for scale compression/stretching in $\delta^{18}O$. We applied an offset correction based on two neighboring ETH-3
537 standards to correct the Δ_{47} sample measurements for long-term variability in the mass spectrometer performance.
538 Then, the data was transferred into the I-CDES by using an empirical transfer function (ETF) that is based on the
539 raw Δ_{47} values of the ETH standards of a window of 4 runs and their InterCarp accepted values at 90 °C acid
540 reaction temperature as determined by ref 63 (ETH-1: Δ_{47} = 0.2052 ±0.0016(1SE)‰; ETH-2: Δ_{47} = 0.2085
541 ±0.0015(1SE) ‰; ETH-3: Δ_{47} = 0.6132 ±0.0014(1SE)‰. To determine final values for both $\delta^{13}C$ and $\delta^{18}O$, an offset
542 correction was applied based on the measured and reported stable isotope values of all three ETH standards in ref
543 25 (ETH-1: $\delta^{13}C_{VPDB}$ = 2.02±0.03‰, $\delta^{18}O_{VPDB}$ = –2.19±0.04‰; ETH-2: $\delta^{13}C_{VPDB}$ = –10.17±0.06‰, $\delta^{18}O_{VPDB}$ = –
544 18.69±0.11‰; ETH-3: $\delta^{13}C_{VPDB}$ = 1.71±0.02‰, $\delta^{18}O_{VPDB}$ = –1.78±0.06‰).
545 The external reproducibility (one standard deviation) of the $\delta^{13}C$, $\delta^{18}O$, and Δ_{47} measurements for each of the
546 standards is listed in the Archive in the Supplementary Data File. Regarding the clumped isotope data, outliers are
547 absent in the successful (no issues with backgrounds, contamination, and/or intensity) sample measurements. The
548 final Δ_{47} values of all these successful measurements are within 4 standard deviations off from the mean. Raw
549 stable and clumped isotope data for all standard and sample measurements are included in the Supplementary
550 Data File.
551

552 **References**

553 73. Kocken, I. J., Müller, I. A. & Ziegler, M. Optimizing the use of carbonate standards to minimize uncertainties
554 in clumped isotope data. *Geochem. Geophys. Geosyst.* **20**, 5565–5577 (2019).
555 74. Schmid, T. W., Radke, J. & Bernasconi, S. M. Clumped-isotope measurements on small carbonate samples
556 with a Kiel IV carbonate device and a MAT 253 mass spectrometer. *Thermo Fisher Application Note* **30233,**
557 (2012).
558 75. Ghosh, P. *et al*. 13C–18O bonds in carbonate minerals: a new kind of paleothermometer. *Geochim.*
559 *Cosmochim. Acta* **70**, 1439-1456 (2006).
560 76. Bernasconi, S. M. *et al*. Background effects on Faraday collectors in gas-source mass spectrometry and
561 implications for clumped isotope measurements. *Rapid Communications in Mass Spectrometry* **27**, 603–612
562 (2013).
563 77. Huntington, K. W. *et al*. Methods and limitations of 'clumped'CO2 isotope (Δ47) analysis by gas-source
564 isotope ratio mass spectrometry. *Journal of Mass Spectrometry* **44**, 1318–1329 (2009).
565 78. Hu, B. *et al*. A modified procedure for gas-source isotope ratio mass spectrometry: The long-integration dual-
566 inlet (LIDI) methodology and implications for clumped isotope measurements. *Rapid Communications in*
567 *Mass Spectrometry* **28**, 1413–1425 (2014).
568 79. He, B., Olack, G. A. & Colman, A. S. Pressure baseline correction and high-precision CO2 clumped-isotope
569 (∆ 47) measurements in bellows and micro-volume modes. *Rapid Communications in Mass Spectrometry* **26**,
570 2837–2853 (2012).
571 80. Dennis, K. J., Affek, H. P., Passey, B. H., Schrag, D. P. & Eiler, J. M. Defining an absolute reference frame
572 for 'clumped'isotope studies of CO2. *Geochim. Cosmochim. Acta* **75**, 7117–7131 (2011).